A bivalent histone mark reader, AtDEK2 governs plant immunity

A bivalent histone mark reader, AtDEK2 governs plant immunity

Naganand Rayapuram

naganand.rayapuram@kaust.edu.sa

KAUST - King Abdullah University of Science and Technology https://orcid.org/0000-0003-2056-3735

Hanna Alhoraibi

King Abdulaziz university

Santiago Alejandro-Martinez

IPS2

David Latrasse

IPS2, CNRS, INRA, Universities of Paris Diderot and Sorbonne Paris Cité

Papita Mandal

KAUST

Lea Faivre

Freie Universitat berlin

Xiaoning He

IPS2

Déborah Manza Mianza

Université Paris-Saclay

Aala Abulfaraj

King Abdulaziz University

Siba Alhrabi

KAUST

Kiruthiga Mariappan

King Abdullah University of Science and Technology (KAUST)

Olga Artyukh

KAUST

Fatimah Abdulhakim

KAUST https://orcid.org/0000-0002-8557-0955

Fatimah Aljedaani

KAUST

Stephan David

KAUST

Marilia Almeida-Trapp
King Abdullah Univ. of Science and Technology
Jean Bigeard
IPS2
Delphine Pflieger
Universite Grenoble Alpes
Wolfgang Fischle
KAUST
Stefan Arold
King Abdullah University of Science and Technology https://orcid.org/0000-0001-5278-0668
Jean Colcombet
IPS2
Daniel Schubert
Freie Universitat Berlin
Moussa Benhamed
Institute of Plant Sciences Paris Saclay https://orcid.org/0000-0002-2716-748X
Ikram Blilou
King Abdullah University of Science and Technology
Heribert Hirt
KAUST - King Abdullah University of Science and Technology https://orcid.org/0000-0003-3119-9633

Article

Keywords: A. thaliana, DEK domain containing protein, Chromatin, Immunity, Epigenetics, Histone modification reader

Posted Date: March 5th, 2024

DOI: https://doi.org/10.21203/rs.3.rs-3829971/v1

Additional Declarations: There is **NO** Competing Interest.

Abstract

In *Arabidopsis thaliana*, the nuclear protein DEK2 orchestrates diverse chromatin-related processes and exhibits phosphorylation in response to flagellin22 treatment, implicating its involvement in plant immunity against bacterial pathogens. Loss-of-function mutants of dek2 have their immunity compromised to both bacterial and fungal pathogens. Transcriptomic analysis of the *dek2-1* mutant unveils AtDEK2 as a transcriptional repressor of defense-related genes, as well as genes associated with hormone synthesis and signaling. Chromatin immunoprecipitation sequencing (ChIP-Seq) analysis reveals that DEK2 binds to motifs of various transcription factor families, with a notable enrichment in class I TCP binding motif regions. Our findings indicate that DEK2 is recruited to specific chromatin regions by transcription factors and functions as a reader of the bivalent histone mark H3K4me3K27me3. Consequently, we propose a hypothetical working model wherein DEK2 acts as a transcriptional repressor targeting regions marked by H3K4me3K27me3, shedding light on its role in plant immunity.

Introduction

Chromatin remodeling plays a pivotal role in the transcriptional regulation of gene expression during development and stress responses in plants[1,2]. One of the non-histone chromatin factors is DEK domain-containing protein. DEKs are abundant non-histone chromatin proteins that are found in multicellular organisms including animals, plants, fungi as well as some single-celled organisms such as Trypanosoma, but they are absent in lower eukaryotes such as yeast and *Caenorhabditis elegans*[3]. This indicates that DEK functions represent an evolutionary requisite for chromatin organization and regulation, which became more complex through evolution[4]. DEKs were originally identified in humans as being part of a fusion protein (DEK-CAN) in a subset of patients with acute myeloid leukemia that is characterized by a specific t(6;9) chromosomal translocation[5,6]. Moreover, DEKs were found in most human tissues and overexpressed in proliferating cells; therefore, DEKs were associated with various types of solid tumors[7–9]. Later, DEKs were identified as an auto antigen in several autoimmune diseases including juvenile idiopathic arthritis[10–12].

Human DEK is a conserved and mostly disordered protein with two domains and no known enzymatic activity or paralogs suggesting stringent evolutionary pressure on this gene[3,13]. Data derived from structural studies by NMR suggest that DEK has two structural domains: a scaffold attachment protein motif (SAF/SAP box) and a C-terminal DNA-binding domain[14,15]. The central SAP domain is a DNA-binding motif that is found in DEK proteins from all organisms and in different chromatin-associated proteins involved in chromatin processes. The SAF/SAP box motif in DEKs is accompanied by a pseudo-SAP box with similar structure and different sequence from the SAF/SAP box. A second DNA binding structure is the carboxy-terminal region that partially overlaps with a multimerization domain. Phosphorylation of the C-terminal region by casein kinase 2 (CK2) reduces its binding to DNA and enhances its multimerization, suggesting phosphorylation as a major mechanism in regulating the function of DEK[16]. Under stress conditions, other post-translational modifications such as acetylation by

p300[17] and poly ADP-ribosylation by PARP1[18] have been identified as critical regulators of its DNA/chromatin binding, localization and biological activity[15].

Different biochemical studies revealed that DEK prefers to bind cruciform DNA *in vitro* and introduces supercoils into dsDNA indicating that DEK might play an active role in maintaining higher-order chromatin architecture[3,19]. Another study suggests that DEK-DNA binding depends on the sequence of the DNA[20]. In addition to its DNA, histone and chromatin binding properties, some studies have reported that DEK interacts with RNA and is involved in RNA processing[21,22]. Therefore, DEK protein is implicated in regulating several nuclear processes including chromatin structure [4,19,23,24], epigenetic modification, transcriptional regulation [25–28], mRNA splicing [21,29], chaperone activity [23,27,30–32], DNA replication and repair [13,33,34].

Recently, the complexity of DEK family members and their functions *in vivo* was further studied in plants. The *A. thaliana* genome encodes four DEK proteins namely DEK1, DEK2, DEK3 and DEK4. Only DEK3 was further characterized by Waidmann *et al*. [35] based on its relatively abundant expression level. Accordingly, DEK3 is a chromatin architectural protein capable of modulating DNA topology, nucleosome occupancy, chromatin accessibility and gene expression. In addition, plants deficient in DEK3 exhibited increased germination efficiency and survival under high-salinity and high-heat conditions compared to WT plants, suggesting that DEK3 is important for the regulation of stress responses[35]. Moreover, DEK3 was found to be enriched in the up- and down-stream regulatory regions of genes resembling the distribution of H3.3 and RNAPII in both *A. thaliana* and animals, which proposes a possible role of DEK as a transcriptional regulator in *A. thaliana* [32,35]. Recently, it was shown that DEK3 is phosphorylated by the salt stress-activated glycogen synthase kinase 3 (GSK3) and this alters the composition of the nuclear protein complex harboring DEK3 and affects nucleosome occupancy and chromatin accessibility[36]. Additionally, it was shown that DEK3 and DEK4 regulate floral transition in *A. thaliana*. Both, DEK3 and DEK4 associate directly with the chromatin of floral repressors FLOWERING LOCUS C (FLC), and its two homologs, MADS AFFECTING FLOWERING4 (MAF4) and MAF5, to promote their expression. Histone modifications at the FLC, MAF4 and MAF5 loci are also affected by the binding of DEK3 and DEK4 to the histone octamer[37].

In a large-scale quantitative phosphoproteomic study DEK2 was found to be phosphorylated in response to flg22 treatment suggesting an important role in plant immunity to bacterial pathogens[38]. Loss of function *DEK2* plants have their immunity compromised to bacterial and fungal pathogens compared to wild type plants. Global transcriptome profiling suggested that DEK2 is a transcriptional repressor. We carried out ChIP-seq analysis and found that DEK2 binds to the regions around the TSS and TES indicating that DEK2 regulates the transcription of its target genes after being recruited by TFs. Additionally, the *dek2* transcriptome profile closely resembled that of a methyltransferase hinting at the possibility of DEK2 being a reader of histone methylation marks. Using a combination of *in silico* and biochemical analyses, we determined that DEK2 preferentially binds to H3K4me3 and H3K27me3 to fine tune the regulation of the target genes.

Results

Isolation and characterization of DEK2 lines

To investigate the role of DEK2 *in vivo*, we obtained two independent T-DNA insertion mutant lines *dek2-1* (SALK_1375152C) and *dek2-2* (SALK_033428) in At5g63550 from the National *Arabidopsis* Stock Center (NASC). The *dek2-1* and the *dek2-2* mutants contain T-DNA insertions in exon 9 and intron 3 of the *DEK2* gene, respectively (Supplementary Fig. 1A). The T-DNA insertion in the *DEK2* gene was confirmed by sequencing. The four-week-old *dek2* mutants showed no developmental phenotype compared to WT plants (Supplementary Fig. 1B). Genotyping of the two mutants using allele specific primers shows that both T-DNA lines are homozygous (Supplementary Fig. 1C).

DEK2 expression levels in the WT and *dek2* mutants were tested by RT-PCR and qRT-PCR. Transcript levels in both *dek2* mutants were reduced compared to WT, indicating that the T-DNA insertion disrupted the expression of the full-length sequence. Thus, both insertion lines are *dek2* loss-of-function mutants (Supplementary Fig. 1D and E). To investigate the expression pattern of *DEK2* in *A. thaliana* plants, we performed histochemical GUS (*β*-Glucuronidase) staining of *DEK2* promoter-GUS lines. *DEK2* promoter activity was detected particularly in the shoot apical meristem, root tip and emerging lateral roots. GUS expression was detectable in the cotyledons but appeared mostly in newly emerging rosette leaves (Supplementary Fig. 1F).

Involvement of DEK2 in plant defense

To elucidate the role of DEK2 in *A. thaliana* immunity, WT and *dek2* T-DNA mutant plants were challenged with the hemibiotrophic bacterial pathogen *Pseudomonas syringae* pv. *tomato* DC3000 *(Pst* DC3000). Plants were spray-inoculated with the virulent bacterium and the number of bacteria was counted at 3 and 48 hours post infection (hpi). There was no change in the bacterial titers at 3 hpi in WT and *dek2* mutants indicating that DEK2 is not involved in stomatal immunity. At 48 hpi, *dek2* mutant plants displayed more disease symptoms than WT. Similarly, bacterial growth in infected leaves of both *dek2* mutants was significantly higher in comparison to WT at 48 hpi (Fig. 1A).

Production of reactive oxygen species (ROS) is a defense hallmark induced by flg22. *dek2-1* mutant shows increased flg22-triggered ROS production compared to WT (Fig. 1B). Callose deposition, another PTI response to limit pathogen attack after flg22 treatment, was also tested in the mutant plants. Although *dek2-1* shows a lower number of callose deposits in untreated conditions, both *dek2* mutants show increased flg22-induced callose deposits (Fig. 1C and D). These data suggest that DEK2 is a key regulator of plant defense to pathogenic bacteria. We then looked at the MAPK activation in the WT and mutant plants and observed that both *dek2* mutant plants are compromised in their MAPK activation in response to flg22 treatment (Fig. 1E).

To test whether the disease phenotypes observed in *dek2* mutant plants are linked to changes in gene regulation, we performed RNA-seq analysis of 14-day-old *dek2-1* mutant and WT plants in untreated

conditions and 24 h after treatment with *Pst* DC3000 *hrcC*. *Pst-hrcC* pathogen has a defect in type III secretion system necessary for the delivery of effectors and therefore it is used for studying PTI. Samples from three independent biological repeats were collected for RNA-seq analysis. In unstressed conditions, among 23639 detectable transcripts, 298 differentially expressed genes (DEGs) (cut-off fold change ≥ 2, P value ≤ 0.05, q value ≤ 0.05) were identified in *dek2-1* mutant compared with WT plants (Supplementary Table 1). Among the DEGs, 63% were upregulated suggesting that DEK2 functions as a repressor of transcription (Fig. 1F). The 184 upregulated genes are enriched in GO terms associated with response to stimulus, response to chitin, response to stress, defense response, response to hormone stimulus and immune response. The 114 down-regulated genes show enrichment in genes involved in photosynthesis, oxidation-reduction and generation of precursor metabolites and energy. Under stress, there were 254 genes down-regulated in *dek2* compared to WT and these genes were enriched in regulation of biosynthesis process and regulation of transcription whereas the 131 up-regulated genes were associated with GO terms including response to stress, defense response and response to wounding.

To further investigate how DEK2 modulates the expression of its target genes, we used a dual luciferase system where DEK2-RFP was expressed under CaMV 35S promoter, *pMYC2* was fused to Firefly-Luc and Renilla-Luc was expressed under CaMV 35S as the internal control. As shown in Fig. 1G, in tobacco leaves, DEK2 was able to repress the expression of Firefly-Luc significantly. TCP20 was used a positive control for the repression of the *pMYC2* activity.

Hierarchical clustering of DEGs in the *dek2-1* mutant and WT in the resting and stress conditions showed a large set of genes which were upregulated in the *dek2-1* mutant compared to the WT without treatment (Fig. 1H). These clusters were sub-grouped into ten clusters based on similarity in transcription between WT and *dek2-1* in the mock and treated conditions. To gain a general overview of the transcriptional changes, we performed a Gene Ontology (GO) enrichment analysis for three of the interesting clusters (Fig. 1H). Cluster II (genes induced in *dek2*-hrcC more than in WT-hrcC) was mainly associated with defense responses and glucosinolate related processes. Interestingly, cluster III (genes induced in *dek2* but not in the WT in the mock and behave oppositely after treatment) was enriched with GO terms involved in responses to hormones and hormone signaling. Many defense-related transcription factors, such as MYBs and ERFs bHLH were over-represented in cluster III. Cluster IX (genes only induced in WT-hrcC) represents genes associated with defense responses, transcription regulation and RNA processes including *ERF6, ERF4, MYB73, MYB15* and *ZAT6*. Collectively, the data suggest that DEK2 might control general gene transcription as a transcriptional repressor.

Hormone metabolism and homeostasis are affected in *dek2*

The RNA-seq-based transcriptome analysis indicated that the expression of a number of genes associated with jasmonic acid (JA) biosynthesis and signaling pathways are affected in *dek2-1* mutant. Consequently, we quantified the levels of three major phytohormones involved in plant responses to

stresses, namely JA, ABA and SA, in WT and *dek2-1* mutant with or without *Pst* DC3000 infection from six biological replicates. In untreated plants, the JA and JA-ile levels were higher in the mutant compared to the control (Fig. 2A) whereas ABA levels were lower in the mutant compared to WT. Upon *hrcC*-treatment, SA levels were remarkably reduced compared to WT. To check if this hormone imbalance was also reflected at the transcriptional level, the expression of genes involved in JA biosynthesis including *LOX, AOC* and *AOS* genes were measured and found to be up-regulated (Fig. 2B). In addition, the ethylene biosynthesis genes, 1-Aminocyclopropane-1-Carboxylic Acid Synthase (ACS), namely *ACS8* and *ACS6* were upregulated in the mock conditions (Fig. 2B). Since JA plays a critical role in necrotrophic fungal infection, we tested the response of *dek2* mutant plants to the necrotrophic fungus *B. cinerea.* After two days of drop-inoculation with $5x10^5$ spores/ml, *dek2* mutants formed smaller necrotic lesions compared to WT plants. This result indicates that *dek2* loss-of-function mutant is more resistant to the pathogenic fungi (Fig. 2C and D).

Determination of DEK2 target sites by ChIP-Seq

We generated complementation lines expressing DEK2-YFP under its own promoter (Supplementary Fig. 2). To determine how DEK2 plays a role in plant immune response, we explored the genomic loci at which DEK2 exerts its activity by chromatin immunoprecipitation-sequencing (ChIP-Seq) using anti-GFP antibody in DEK2-YFP expressing lines and mapped the datasets to the *A. thaliana* genome. The experiments were performed on two-week-old seedlings comparing WT expressing GFP and *dek2-1* complemented by *pDEK2::gDEK2:YFP* from three biological replicates. The majority of the binding sites of DEK2-YFP remarkably covered the region surrounding the transcription start site (TSS) as well as the region of transcription end site (TES), suggesting the involvement of DEK2 in transcription (Fig. 3A). The maximum enrichment was found in the upstream promoter region compared to other regions (Fig. 3B). The ChIP-Seq data identified 4269 high confident binding sites for DEK2-YFP associated with 4253 genes in the *A. thaliana* genome (Supplementary Table 2). Through the use of the MNase-seq experiment on wild-type plants, we were able to identify MNase hypersensitive sites and investigate further the link between nucleosome regions and DEK2-YFP enriched loci. Using this technique, we discovered that in wild-type seedlings, the DEK2-YFP peaks primarily exhibit an anti-correlation with nucleosomal occupancy (Fig. 3C). Additionally, we used an ATAC-seq (assay for transposase-accessible chromatin utilizing sequencing) method, which enables nuclesosome-free regions (NFRs) to be precisely positioned. Remarkably, testing showed that NFR profiles and DEK2 placement around the TSSs correlated perfectly (Fig. 3D). Together, these results revealed that DEK2 is commonly enriched over hundreds of genes' 5' NFR, which is consistent with DEK2 possibly having a direct impact on local transcriptional regulation. We investigated the correlation between DEK2 enrichment and mRNA levels in order to comprehend the link between DEK2 and gene expression. This showed that the quantity of transcripts at particular loci and the binding frequency of this protein were positively correlated (Fig. 3E). We postulated that DEK2-association was with particular DNA-sequence motifs rather than chromatin markers because DEK2-YFP distribution is enriched over NFRs. The G-box consensus sequence TGGGCC was shown to be an over-represented cis element inside the DEK2 peaks by *de novo* motif finding using the HOMER software (Fig. 3F). It is known that this motif recruits several transcription factors, including bZIP and WRKY.

DEK2 is recruited by transcription factors (TFs) to target sites on the DNA

In order to confirm the binding of DEK2 to the TCP DNA motif, we carried out electrophoretic mobility shift assay (EMSA) by incubating purified recombinant His-MBP-DEK2 with a biotin-labeled TCP binding DNA probe. DEK2 did not bind to the probe while the positive control used for the assay showed proper binding (Supplementary Fig. 3). Since the ChIP-seq experiments showed several binding sites corresponding to different TFs, we hypothesized that DEK2 is recruited by the TFs to the target sites on the DNA. To test this hypothesis and since class I TCPs were the most prominent group of TFs, we tested the binding of DEK2 with TCPs. Using yeast two-hybrid (Y2H) assay, we tested the interaction of DEK2 with 6 different class I TCPs – TCP8, TCP9, TCP15, TCP19, TCP20 and TCP21 and found that DEK2 interacts with a few TCPs but most strongly with TCP20 (Fig. 3G). The positive and negative controls for TCP20 are shown in panel G. To further confirm this interaction, we carried out bimolecular fluorescence complementation with TCP20 and DEK2 to demonstrate that the two proteins do interact with each other (Fig. 3H). However, the targets of DEK2 and TCP20 showed very little overlap suggesting that TCP20 also regulates a number of genes independently of DEK2 (Fig. 3I). The peaks of IP samples are higher than those of the input, indicating clear DEK2-binding regions of the target genes. Among these common genes were *MKK9*, *ERF1*, *ERF6*, *WEI2*, *PBL39* that are known to mediate defense responses. The regulation of ACS6, which is involved in ET biosynthesis pathway is known to occur via the MKK9-MPK3 pathway that activates WRKY33 and ultimately induces the expression of *ACS6*.

DEK2 is a reader of bivalent histone methylation marks

The RNA-seq data strongly suggest that DEK2 acts as a transcriptional repressor of different sets of genes that are primarily involved in plant defense against bacterial pathogens. Therefore, we looked for the most similar transcriptome profiles in the *A. thaliana* database using the signature tool of Genevestigator, which compares the global expression levels of an experiment of interest to a subset of other global transcriptome profiles with similar gene responses. Interestingly, when we compared the transcriptome profile of *dek2-1* with the ones found in the repository, *dek2-1* showed highest similarity to the triple mutant of TRITHORAX-RELATED PROTEIN 5/6 (*atxr5/6)* and MORPHEUS' MOLECULE 1 mutant (*mom1*) (Supplementary Fig. 4).

ATXR5 and ATXR6 function as methyl transferases of H3K27me1 in *A. thaliana*, therefore we hypothesized that DEK2 might act as a reader of histone methylation marks. The binding of DEK2 to H3K4, H3K9, H3K27 methylation marks may represent its ability to target or read these histone methylation marks.

DEK protein orthologues of Human and Drosophila have been shown to interact with histones[23,24,32]. More recently *A. thaliana* DEK3 and DEK4 were also shown to be interacting with histones[35,37]. To investigate if DEK2 also binds to histones, we incubated His-MBP-DEK2 bound Ni-NTA beads with histones purified from calf thymus and then after resolving the proteins by SDS-PAGE and western

blotting, we probed the blot with antibodies against H2A, H3 and H4. DEK2 interacted predominantly with H3 and to some extent with H4 but not with H2A (Fig. 4A).

To further examine the binding of recombinant *A. thaliana* His_6-MBP-DEK2 protein with differentially methylated histone H3 peptides, we employed both quantitative peptide pull-down assays and microscale thermophoresis (MST). Both the assays showed that DEK2 failed to recognize the singly modified H3 peptides (Fig. 4B, C and Supplementary table X). Only a weak binding was observed with H3K9me1 peptide with a Kd around 304 µM. A histone H3K9me3 binding protein UHRF1 [39] was used as a positive control in the binding assay.

However, the chromatin is a complex environment characterized by the co-existence of numerous histone modifications on a single or neighboring nucleosomes. Indeed, certain readers were shown to recognize a combination of modifications rather than a single one such as the human BPTF that binds H4K16ac, in combination with H3K4me3[40] and the rice CHD3 protein CHR729 that bind H3K4me3 and H3K27me3[41]. To probe whether DEK2 might recognize a specific combination of chromatin marks, an *in silico* chromatin state analysis was performed using the chromatin topology established by Sequeira-Mendes et al.,[42]. When examining the overlap between DEK2-bound sequences and the different chromatin states, we could observe a strong enrichment both for chromatin states 1 and 2. Chromatin state 1 is found mostly on promoters and gene bodies and is enriched in active marks such as H3K4me2, H3K4me3 and H3K36me3 while chromatin state 2 is mostly found on promoters and is characterized by the simultaneous presence of the antagonistic marks H3K27me3 and H3K4me3. The preferential localization of DEK2 on state 1 and 2 loci suggests that DEK2 might recognize activating marks such as H3K4me2 or 3 which are found in both chromatin states, or the bivalent H3K4me3-H3K27me3 chromatin state (Fig. 4D).

As DEK2 can act as a repressor or an activator on its target genes, we investigated whether its target genes could be linked to the specific chromatin states. We therefore segregated the DEK2 target genes into three categories depending on the impact of the absence of DEK2 on their transcriptional levels and examined their chromatin state. We found that all DEK2 target genes are enriched in State 1, regardless of the role of DEK2 on their transcriptional regulation. However, only the genes which are upregulated in the *dek2* mutant showed an enrichment in State 2, suggesting that DEK2 might act as a transcriptional repressor of certain bivalent genes (Fig. 4E) which are enriched in H3K4me3K27me3 histone marks.

To confirm the *in-silico* analyses, we performed the binding assays of recombinant *A. thaliana* His_6-MBP-DEK2 protein with H3K4me2, H3K4me3, H3K27me2, H3K27me3, H3K4me3K27me3 histone peptides. DEK2 specifically recognized the bivalently modified peptide H3K4me3K27me3 with a Kd of ~ 65 nM (Fig. 4F and Table 1).

Table 1. Binding affinities of H3 Peptides

H3 peptides	Binding affinities (Kd) for DEK2
H3K4me3	nb
H3K9me1	~ 304 ± 13
H3K9me2	nb
H3K9me3	nb
H3K27me1	nb
H3K27me2	nb
H3K27me3	nb
H3K4me3K27me3	65 ±3.4

As the chromatin states defined by Sequeira-Mendes et al.,[42] are generated by combining ChIP-seq datasets generated by distinct studies and both H3K4me3 and H3K27me3 distributions are known to be highly dynamic during development but also the day-night cycle[43,44], it was crucial to verify that both marks actually co-occur at the same time on DEK2 target genes. We, therefore, performed separate ChIP with H3K4me3 and H3K27me3. While the levels of each mark varied slightly depending on the gene, all putative bivalent DEK2 targets tested showed an enrichment in H3K4me3 and H3K27me3 at the same locus, reinforcing the idea that those genes might be bivalent and that DEK2 might act as a bivalency reader.

Discussion

To defend against a multitude of biotic aggressors, plants have evolved a plethora of complex immune response pathways which enable them to cope with such adverse conditions[45]. PAMP recognition by plant receptors activates signal transduction by MAPK signaling cascades leading to transcriptional reprogramming of defense-related genes and PAMP-triggered immunity responses. Research over the last decades has identified important transcription factors and chromatin-related proteins targeted by immune MAP kinases to regulate transcriptional re-programming of immune-related genes[46]. Some of these immune MAPK targets are involved in chromatin modification and remodeling in *A. thaliana*. For example, flg22-activated MPK3 directly interacts and phosphorylates histone deacetylase (HD2B) to regulate the reprogramming of defense gene expression and innate immunity through modulation of the H3K9ac histone mark[47].

DEK2 was identified from chromatin phosphoproteomics as a protein that gets phosphorylated upon flg22 treatment[38]. The *in vivo* flg22-induced phosphorylation of DEK2 on S238 was compromised in *mpk6* mutant suggesting that DEK2 is a MPK6 substrate. Recently, DEK3 was shown to be phosphorylated by GSK3 altering nucleosome occupancy and chromatin accessibility[36]. Furthermore, in humans, non-phosphorylated DEK binds to DNA and this DEK-DNA binding is weakened by the phosphorylation of the C-terminal DEK domain by casein kinase 2 (CK2)[16]. These studies show that

phosphorylation of DEKs occurs in plants and humans and suggests that further investigations are warranted to clarify the role in chromatin regulation.

The presence of multiple DEK genes in plants compared to other eukaryotic genomes which have only one paralog might be due to gene duplication events during plant evolution to acquire novel gene functions that contribute to improved vigor and adaptation to adverse environmental conditions[48]. Extensive studies in other higher eukaryotes reported DEK as a chromatin related protein that regulates different chromatin related processes. In contrast, the functions of DEKs in plants are less understood. A study on a member of the *A. thaliana* DEK family, DEK3, showed that this protein specifically interacts with histones H3 and H4 and regulates nucleosome occupancy and chromatin accessibility. The study further showed that DEK3 plays a negative role in regulating salt-stress by modulating the expression of downstream target genes relevant to abiotic stress responses[35]. In our phosphoproteomics study, DEK2 was phosphorylated in response to PAMP treatment suggesting that DEK2 might play a significant role in biotic stress. To test this hypothesis, we performed pathogen assays on WT and *dek2* loss-of-function mutants and observed that *dek2* mutants are more susceptible to both bacterial (*Pst* DC3000) and fungal (*B. cinerea*) pathogens. In addition, the *dek2* mutant plants were also found to be deregulated in the generation of ROS and callose deposits after PAMP treatment compared to WT. Taken together, these results indicate that DEK2 plays a crucial role in plant immunity.

Under unstressed condition, the majority of DEGs in *dek2* mutant were up-regulated compared to WT, including many hormone biosynthesis pathway genes and transcription factors. These data indicate that DEK2 acts as a general transcriptional repressor as was shown for DEK3[35]. To understand how DEK2 regulates the expression of these genes and investigate the global distribution of DEK2 on the genome, we performed ChIP-seq with DEK2:DEK2-YFP plants. ChIP-Seq analysis showed that DEK2 binding was highly enriched in regions around TSS and TES. To correlate DEK2 binding to changes in gene expression, ChIP-seq results were compared to the transcriptome of the *dek2* mutant to find the direct target genes and potential binding sites of DEK2 in these chromatin regions. DEK2 binds to PCF motif consensus sequence TGGGC(C/T) to regulate transcription. The PCF/TCPs are transcription factors with a conserved bHLH motif, called TCP domain[49–52]. The 24 TCPs encoded by the *A. thaliana* genome are divided into two classes, class I with 13 members and class II with 11 members, which are proposed to act antagonistically[53,54]. Beside their function as classical developmental regulators, several studies have shed light on the role of TCP proteins in plant immunity via stimulating the biosynthetic pathways of bioactive metabolites including BR, JA and flavonoids[55–62]. Hs-DEK and Dm-DEK proteins interact with histones and play a role in nucleosome assembly and DEK3 was implicated in similar processes at DEK3 target sites in *A. thaliana*. These data strongly enforce DEK3 as a histone chaperone[23,24,35].

Additionally, the global transcriptome profile of untreated *dek2* mutant shows a similarity to that of *atxr5/6/mom1* triple mutant. Previous studies have identified ATXR5 and ATXR6 as monomethyl transferases of H3K27[63] while MOM1 is a component of a silencing machinery of highly repetitive sequences independent of DNA methylation marks[64,65]. Mutations in *atxr5* and *atxr6* lead to

transcriptional activation of repressed heterochromatic elements whereas mutation in *MOM1* releases transcription gene silencing independently of the epigenetic markers[63]. Previous studies indicated that different stresses can mediate changes in chromatin structure and therefore initiate transcriptional stress responses[66,67]. In *A. thaliana*, DEK3 is crucial for abiotic stress tolerance[35]. Histone post-translational modifications such as acetylation, methylation, phosphorylation, ubiquitination, sumoylation, carbonylation and glycosylation represent an important level in epigenetic regulation[68,69]. Depending on their targets, histone methylation on histone tail can either activate or repress transcription. For example, *A. thaliana* H3K4me3 and H3K36me3 are associated with gene activation whereas H3K9me1/2 and H4K20me1 are enriched at constitutive heterochromatin and silenced transposons and H3K27me3 is associated with repressed genes[70,71]. The regulation of gene activity requires different writers, readers and erasers of histone methylation[72]. Our *in silico* analysis and biochemical binding analysis shows the preferable binding of DEK2 to bivalent histone marks H3K4me3 H3K27me3 compared to other histone methylation marks. ChIP-PCR of a few DEK2 targets with H3K4me3 and H3K27me3 antibodies confirms that DEK2 indeed binds to chromatin states with these bivalent histone marks. The data suggest that DEK2 acts as a reader that specifically binds to H3K4me3K27me3 marks in *A. thaliana*. The known reader of H3K9me3 from fission yeast to mammalian is heterochromatin protein 1 (HP1) that recognizes H3K9me3 through its conserved chromodomain and maintains heterochromatin formation[73,74]. *A. thaliana* LIKE HETEROCHROMATIN PROTEIN 1 (LHP1), the homolog of HP1, recognizes H3K27me3 and resembles Polycomb proteins[75,76]. A paper by Zhao et al. identified Agenet Domain Containing Protein 1 (ADCP1) as a multivalent H3K9me reader in plants[77]. In *A. thaliana*, only EBS and SHL were described as bivalent readers, but contrary to DEK2, they could also bind peptides carrying only K4me3 or only K27me3[78,79]. This would make DEK2 the first plant reader that specifically binds to K4me3K27me3.

Based on all the data obtained, we propose a hypothetical working model (Fig. 5). Under unstressed condition (Fig. 5A), DEK2 is recruited by TFs and thereby regulates the expression of the target genes. This is supported by the transcriptome data of *dek2* that show that the majority of genes are upregulated in *dek2* mutant. Upon pathogen attack or PAMP treatment, DEK2 might disassociate from the DEK2-TF complex, and as a consequence, drives the expression of target genes (Fig. 5B). DEK2, which according to our data functions as a reader of H3K4me3k27me3 marks, adds another layer of specificity to the regulation of transcription and epigenetic control.

Materials and methods

Plant materials and growth conditions

A.thaliana Columbia accession (Col-0) was used as wild-type plant in this study. The DEK2 T-DNA insertion mutants *dek2-1 (SALK_1375152C)* was provided by Claudia Jonak and *dek2-2 (*SALK_033428) was obtained from the Nottingham Arabidopsis Seed Centre (NASC) and genotyped by PCR for homozygosity.

A. thaliana seeds were surface sterilized in a solution of bleach: ethanol: H_2O (V:V:V::1:4:3) for 10 min and washed four times with sterile water. The seeds were then stratified by placing them at 4°C for 48 h. Seedlings were grown on 1/2 MS plates in a plant growth chamber for 14 days at 21°C with 75% relative humidity under 16 h of daylight. *A. thaliana* plants were grown on Jiffy-7 pots to prevent contaminations from garden soil for four weeks at 23°C, 60% relative humidity with an 8 h light/16 h dark short-day photoperiod and 16 h light/8 h dark long day photoperiod in environmentally controlled growth cabinet (Percival). 2g/L of fertilizer were added on the second and fourth weeks. *N.benthamiana* plants were grown in the green house under these conditions: humidity 70%, temperature 28°C, long day.

Pathogen strains and growth conditions

Escherichia coli (E. coli) bacteria was grown on LB broth or agar medium for cloning and protein expression purposes. The bacterial pathogen *Pseudomonas syringae pv. tomato DC3000 (Pst DC3000*) and *hrcC*$^{-}$ mutant (defective in type III secretion system) strains were grown on NYGA agar medium supplemented with 50 mg/ml rifampicin at 28°C for 48h for infection assay hormone quantification and RNA-seq experiment. *Agrobacterium tumefaciens* (*C58C1*) was grown in 10 ml LB medium with appropriate antibiotics overnight at 28°C for generating transgenic lines and transient expression studies. The necrotrophic fungus B*otrytis cinerea* strain BS05.10 was grown on potato dextrose plates at 22°C for two weeks in dark.

Plant transformation of A. thaliana by floral dip method

About five-week-old *A. thaliana* plants were grown under long days in pots. The transformation was done with *Agrobacterium tumefaciens* (*C58C1*) by using the floral dip method[80]. Transgenic plants were selected on MS agar with appropriate selection agent (BASTA 100 µg/mL, Hygromycin 10 µg/mL). Genotypes of survival transgenic plants were validated by PCR in the T1 generation, and confirmed in the following 2–3 generations. For all the transformation, four transgenic lines were obtained and were used for phenotypic analysis.

Infection of A. thaliana with Pseudomonas syringae pv. tomato DC3000

Pseudomonas syringae pv. *tomato* DC3000 (*Pst* DC3000) bacteria were resuspended in 10 mM of $MgCl_2$ in the presence of 0.04% Silwet L-77 and adjusted to OD600 = 0.2. Four-week-old *A. thaliana* plants were spray-inoculated with *Pst* DC3000 bacteria and the bacterial growth was quantified as described earlier[38]. The infection assays were repeated three times with reproducible results.

Infection of A. thaliana with Botrytis cinerea

The necrotrophic fungus *B.cinerea* was cultivated for 14 days and spores were collected in Vogel buffer (for 1 L: 15 g of Sucrose, 3 g of Na-citrate, 5 g of K2HPO4, 0.2 g of MgSO4·7H2O, 0.1 g of CaCl2·2H2O, and 2 g of NH4NO3) as previously described[81]. Spore number was determined using a hemocytometer and adjusted to a final conc of 5×10^5 spores/ml. Five leaves of four-week-old plants were drop

inoculated with 5 µL of the spore suspension and the trays were cover to maintain humidity. 6–8 plants were used per genotype. Photographs were taken two days after inoculation, and the lesion diameter/area was determined using ImageJ software.

Oxidative burst Measurement

Luminol-HRP-based luminescence method was carried out to quantify ROS in treated leaves. Briefly, 4-mm leaf discs from four-week-old *A. thaliana* were floated in 150µL dH_2O overnight in a 96-well plate in continuous light. Water was then replaced by 100 µl of elicitation reaction mixture containing 1 µM flg22 (QRLSTGSRINSAKDDAAGLQIA) synthesized peptide by GenScript or 100 µM chitin from shrimp shells (Sigma, C9752), 170 µg/ml luminol (Sigma, A4685) and 100 µg/ml horseradish peroxidase (Sigma, P6782). Addition of the same solutions without flg22 or chitin served as controls. Plates were placed immediately into Promega GloMax navigator plate reader and luminescence was recorded at one min intervals over 40 min. Every time point is the mean value of 8 seedlings.

β -Glucuronidase (GUS) staining and subcellular localization

To study the in planta expression of AtDEK2, 1 kb of the promoter region of DEK2 was PCR amplified from RIKEN TAC clone (pdg02820) and cloned into pENTR-D/Topo (Invitrogen) and consequently recombined with the pGWB433 vector by LR reaction to generate *ProAtDEK2*::*Gus construct. The* construct was introduced into *A. thaliana* (Col-0) by Agrobacterium tumefaciens-mediated transformation C58C1. Progeny of these transgenic plants were selected on MS agar plates supplemented with 50 µM kanamycin. Histochemical detection of GUS activity was performed using 5–10 day-old seedlings incubated in the GUS staining solution as described in[82] at 37°C for 1–3 hours followed by destaining in Visikol (Phytosys LLC).

Subcellular localization assay was performed on 6-day-old *AtDEK2* transgenic *A. thaliana* complemented stable lines under native promoter fused to YFP. For Subcellular localization in *N. benthamiana*, the gene of interest was cloned in fusion with GFP at their N- or C-terminal part under the control of the CaMV-35S promoter (in the pGWB5 vector), or under the control of ubiquitin promoter in the pUBIN-GFP, pUBIC-GFP respectively. Plasmids were transformed into *A. tumefacies C58C1 and* CFP–serrate as a marker for nucleus were infiltrated into leaves of four-week-old *N. benthamiana* plants using needle less syringes. After three days, fluorescence signals were excited at 488 nm and detected using an upright Zeiss LSM880 laser scanning confocal microscope with a 20X/40X objective (Plan-Apochromat, NA 1.0). All images were acquired using Argon laser.

Bimolecular fluorescence complementation (BiFC)

BiFC was used to visualize the protein-protein interaction and determine the subcellular localization of the interacting proteins. The three MAPKs and the proteins of interest were fused to the N- or C- terminal fragment of YFP that produces a fluorescent readout upon reconstruction of YFP. In the pBIFC1, 2, 3 and 4 vectors used, the expression is under the control of the cauliflower mosaic virus 35S (CaMV-35S) promoter. To test interaction between two proteins by BiFC, eight different combinations of N- or C-

terminally tagged YFP fragments were tested. Appropriate positive and negative controls were carried out for all combinations. The constructs were transiently expressed in *N.benthamiana* leaves by co-infiltration with *Agrobacterium*. To visualize the fluorescence of the reconstituted YFP expression in leaves, an upright Zeiss LSM880 laser scanning confocal microscope with a 20X/40X objective (Plan-Apochromat, NA 1.0) was used and all images were acquired using Argon laser with 514-nm excitation.

Quantification of Phytohormones

Plant hormones (ABA, JA and SA) were extracted and quantified as previously reported[83]. Four-week-old *A. thaliana* plant were harvested 24h after spray inoculation either with 10mM of $MgCl_2$ containing 0.04% of Silwet L-77 as control or infected with *Pst DC3000 hrcC*$^-$ pathogen as described above. Subsequently, plant materials were lyophilized and ground in a Gino grinder (for 2 cycles of 45 sec each, at 1150rpm). 10 mg of plant materials were weighed and extracted with 1 mL of extraction solution containing 70% methanol and the respective phytohormone internal standards (d6-ABA, d6-JA, and d4-SA). Five replicates were prepared for each condition. Extraction procedure and hormone quantification were performed as described[84]. Samples were analyzed using an Agilent 1100 HPLC system (Agilent Technologies, Böblingen, Germany) connected to a LTQ Ion trap mass spectrometer (Thermo Scientific, Bremen, Germany), and the quantification of phytohormones was based on a calibration curve using original SA, JA and ABA standards.

flg22-induced callose deposition

Fourteen day old *A. thaliana* seedlings were grown on ½ MS agar plates and then transferred to ½ MS liquid medium in 12 wells plate before treating with water as control or 1 µM flg22 as a PAMP for 24 h. Then seedlings were fixed in acetic acid: ethanol (1:3 v/v) over night, rehydrated with ethanol (50% v/v) for 1 h, ethanol (30% v/v) for 1 h and then twice with sterilized H_2O. Cleared seedlings were stained with 0.01% aniline blue dissolved in 150 mM K2HPO4. Stained leaves were mounted using 50% glycerol and imaged under a UV microscope (Nikon). Callose deposits were estimated after processing the images by Photoshop and ImageJ software (http://rsb.info.nih.gov/ij/). Six seedlings were analyzed for each treatment.

Isolation of RNA from Plant Tissue

50–100 mg of *A. thaliana* plant leaves or 14 days old seedling grown on ½ MS plates were taken in 2 ml tubes containing 2 steel beads, frozen in liquid Nitrogen and homogenized 2X using a Tissue Lyser (Eppendorf) for 1 min at 20 Hz to obtain a fine powder. NucleoSpin® Plant RNA kit (Macherey Nagel, 7740949) was used to extract the total RNA from the plant. The procedure was performed according to the manufacturer instructions. The final RNA was eluted in 60 µl of RNAse free water. Finally, the RNA was quantified using Nanodrop and the to assess the purity, the ratio of A260/A280 > 2.0 was considered. The RNA was flash frozen in liquid Nitrogen and stored at -80 ^oC to prevent degradation.

cDNA synthesis and qRT-PCR analysis

Reverse transcription was performed using SuperScript™ III First-Strand Synthesis SuperMix (Invitrogen 18080400). The amount of starting material can vary from 0.1pg to 5µg of total RNA and the procedure was performed according to the manufacturer's protocols. The normalized complementary DNA (cDNA) was used for qRT-PCR reactions. qRT-PCR was carried out on the CFX96/CFX384 real-time PCR machine (Bio-Rad) using SsoAdvanced Universal SYBR® Green Supermix (Bio-Rad,172–5270) with the following parameters: 50^{o}C for 2 min, 95^{o}C for 10 min, 39 cycles at (95^{o}C for 10 sec, 60^{o}C for 40 sec) and 65°C for 30 sec to obtain the melting curve. The qRT-PCR was performed using gene-specific primers listed in the Supplementary Table S3, with *A. thaliana* Actin (AT3g18780) and ubiquitin (At4g05320) as internal references for normalization. The resulting data was then analyzed using CFX software and values were normalized to WT. Relative expression levels of genes of interest were calculated using the 2 − ΔΔCT method. qRT-PCR experiments were repeated in three independent biological replicates, each with three technical replicates.

RNA-seq

mRNA libraries were prepared using the illumina Truseq Stranded mRNA Sample Preparation LS (low sample) kit following the manufacturer's protocol. Briefly, the mRNA was purified from 1ug of total RNA using poly-T oligo-attached magnetic beads then purified, fragmented and primed. Subsequently, both first and second strands of cDNA were synthesized using SuperScript II reverse transcriptase, followed by adenylation on the 3' ends and ligation of adapters. The DNA fragments with adapters were amplified by 15 PCR cycles. Finally, the libraries were validated using the 1000 DNA kit on 2100 Bioanalyzer (Agilent Technologies), quantified using qubit (Life Technologies) then barcoded libraries were normalized and pooled in equal volumes. Stranded mRNA libraries were sequenced on an Illumina Hiseq 4000 system using paired-end method. The length of the read was around 150 bp. The RNA-seq was done on three independent biological replicates.

Approximately 40 million reads were obtained for each sample. Reads were quality checked using FASTQC v0.11.5[85]. Adapters and reads with low sequencing quality were filtered using Trimmomatic 0.36[86], retaining first 100 bps and by using other default settings for paired-end sequences. The trimmed reads were then aligned to the *A. thaliana* reference genome (TAIR10) using Tophat v2.1.1[87–89] with –N 2 –g 1. The annotation file was provided as reference for reads alignment. MultibamSummary from deepTools2 package[90] was used on the bam files derived from the previous step, to check for the correlation between the replicates. Summary of read counts at gene level was calculated using feature Counts v1.5.1[91]. Cufflinks v.2.2.1[89] was used to calculate the FPKM values for individual replicates and CuffDiff v2.2.1 with quartile normalization to find the significant differential gene expression[89]. Genes with 2-fold change and P value < = 0.05 were considered as significantly different between samples with and without treatment. Hierarchical clustering of these genes was performed using Mev v4.8.1[92]. GO term enrichment in each gene list was carried out using AgriGO[93] with a cutoff for significant enrichment is P value < 0.01 and calculation false discovery rate < 0.5.

Dual-luciferase transient expression analysis in tobacco leaves

The transcriptional repression activity of DEK2 was assayed using a dual-luciferase transient expression system in tobacco (*Nicotiana benthamiana*) leaves as described[94]. Briefly, pMYC2 was fused to a Firefly Luciferase reporter gene, the regulator/effector (DEK2 and TCP20 as positive control) were fused to RFP and expressed under a CaMV 35S promoter. The expression of RFP was used to confirm the expression of the regulator/effector. Renilla-Luciferase expressed under the CaMV 35S promoter was used to normalize the transformation efficiency. The reporter and effector constructs were introduced into *Agrobacterium tumefaciens* strain GV3101 by electroporation. The transformed Agrobacterium cells were injected into the abaxial side of 4-week-old tobacco leaves using a 1 ml syringe. After 48 hours, D-luciferin substrate was sprayed on the leaves and the reporter gene activity was measured using a CCD Luminescence camera and images acquired.

Recombinant protein expression in E. coli and purification

10ml of an overnight culture of *E. coli* BL21-AI or Rosetta harboring His_6-tagged, His_6-MBP-tagged, GST-tagged proteins or constitutively active MAPKs were diluted in 500 mL LB medium. The culture was grown at 37°C until the OD_{600} reached 0.8, and then induced with L-Arabinose (Sigma, A3256) for BL21-AI cells or 0.5 mM IPTG (Invitrogen 15529-019) for Rosetta cells at 20°C and incubated overnight. Cells were harvested by centrifugation at 4000×g at 4°C for 15 min. The bacterial pellet was resuspended in 40 ml of lysis buffer (50 mM NaH_2PO_4, 300 mM NaCl, 10mM NaCl, pH 8) containing a protease inhibitor cocktail (Complete mini EDTA-free, Roche, 4115449). The cells were lysed by treatment with 2 mg/ml of lysozyme (Thermo scientific, PI89833) for 1 hour on ice, followed by sonication (Branson Digital Sonifier 250–450, runtime 3 min, amplitude 20%, pulse on 2 sec, pulse off 1 sec). The cell lysate was then centrifuged at 20,000xg at 4°C and the supernatant was purified using glutathione sepharose 4B beads (GE Healthcare,17-0756-01) for purification of GST-tagged proteins or Ni^{2+}-NTA beads (Invitrogen, R901-15) for the purification of His-tagged proteins. The proteins were purified according to the manufacturer's protocol. The eluted protein was desalted on PD-10 Desalting columns (GE Healthcare, 17-0851-01). Laemmli 2X protein loading dye (0.5M Tris-HCl pH 6.8, 20% Glycerol, 4% SDS, 2% β-Mercaptoethanol and 0.01% bromophenol blue in distilled water) was added to 20ul of proteins and heated for 10 min at 95°C before analysis on SDS PAGE.

SDS PAGE and Western blotting

The denatured proteins were resolved on a 10% SDS–polyacrylamide gel for 1h at 100V. PageRuler™ Prestained protein marker (Thermo Scientific, 26616) was used as a size standard in SDS-PAGE and western blotting. The gel was stained with Coomassie SimplyBlue Safe Stain (Life Technologies, LC6065).

For Western blot analysis, proteins were transferred from a gel to an ethanol-activated PVDF membranes (GE Healthcare) in a transfer apparatus for 1 h at 100 V. Subsequently, blots were blocked in 5% skimmed milk in Tris buffered saline with tween 20 (1X TBST) (20mM Tris HCL pH7.5, 150mM NaCl, 0.1% tween 20) for 1 hour followed by incubation with the appropriate primary antibody in 2% skimmed milk on a shaker at 4°C overnight. Blots were then washed three times in 1X TBST and appropriate HRP-conjugated secondary anti-rabbit or anti-mouse antibodies were added. Blots were washed again three times in TBST. The blot was visualized using chemiluminescence (ECl prime detection reagent (GE Healthcare, RPN2232) on an imaging system (ChemiDoc MP Bio-Rad). Equal loading was verified by staining the blot with Ponceau S solution (Sigma; P7170).

Chromatin immuno-precipitation (ChIP)

ChIP seq was performed as described in [47]. Briefly, ChIP was performed on 14-day-old seedlings (grown in short day condition, in ½ MS agar plates) using anti-GFP (Santa Cruz). ChIP was performed as previously described[95]. Briefly, plant materials were cross-linked with 1%(v/v) formaldehyde under vacuum. Chromatin was isolated and fragmented by sonication (30 sec on/off pulses, at high intensity for 60 min) using a water bath Bioruptor UCD-200 (Diagenode, Liège, Belgium) Later, the sonicated protein/DNA was incubated with antibodies (overnight at 4°C with gentle shaking) and then incubated with 50 µL of Dynabeads Protein A (Invitrogen, Ref. 100-02D) for 1h at 4°C. Immunoprecipitated DNA was then recovered by dissociating the complexes using the IPure kit (Diagenode, Liège, Belgium) and analyzed by RTqPCR. An aliquot of untreated sonicated chromatin was kept as a total input DNA control.

For ChIP-seq, libraries were prepared and sequenced as described in [96]. ChIP-Seq reads were aligned to *A.thaliana* genome TAIR10 by Bowtie[97] v0.12.7 on *A. thaliana* genome TAIR10. MACS (Model-based Analysis of ChIP-Seq) was used to identify peaks using a q-value cutoff of 0.05 (http://liulab.dfci.harvard.edu/MACS/)[79] while GPAT was used for gene annotation and peak distribution relative to annotated *A. thaliana* transcription start site (http://bips.u-strasbg.fr/GPAT/Gpat_home.html).

Microscale thermophoresis (MST)

Fluorophore-labeled protein was used for the quantitative binding assay using microscale thermophoresis. His6-MBP-DEK2 and His6-MBP (used as control) protein were labeled using Monolith His-tag labeling kit RED-tris-NTA (nanotemper; MO-L008) following the manufacturer's protocol. Briefly, 400 nM of the protein of interest was incubated with 100 nM of the His-tag labeling dye in MST buffer (20 mM HEPES; pH 7.9, 150 mM NaCl, 0.05% Tween-20) for 30 min at room temperature.

The fluorophore-labeled protein was titrated with differentially modified histone H3 peptides (H3K4me1/3, H3K9me1/3, H3K27me1/3). The data points obtained from three different measurements were fitted using the following equation derived from law of mass action to get the dissociation constant:

$$[BL]/[B0] = [([L0]+[B0]+Kd) - \sqrt{(([L0]+[B0]+Kd)^2 - 4\cdot[L0]\cdot[B0])}]/\ 2[B0]\}$$

K_d is the dissociation constant, $[B_0]$ is the total concentration of the binding sites. $[L_0]$ stands for the amount of added ligand at each data point and [BL] is the concentration of formed complexes between the binding sites, [B], and the ligand, [L].

Chromatin states analysis DEK2

The chromatin state analysis was based on the topology established by Sequeira-Mendes et al.[37]. The genomic coordinates of the chromatin states were overlapped with the DEK2 peaks identified as previously described. A DEK2 binding site was considered to be in a certain chromatin state if it overlapped with a domain of that state for at least 150bp. This was tested using the Genomic Ranges package (version 1.44.0)[98]. The control sets were generated by shifting the coordinates of the DEK2 binding site up- or downstream by the indicated number of base pairs. The significance was tested by a permutation test using the peakPermTest() function from the ChIPpeakAnno package (version 3.26.0)[99] with 1000 permutations.

For the DEK2 target genes analysis, the DEK2 targets identified as described previously were divided into 3 sets depending on whether they were up- or downregulated or did not present a change in expression in the *dek2* mutant. A gene was considered as being in a certain state if at least 150 bp of its gene body overlapped with said state. For each chromatin state, the lists of DEK2 targets were overlapped with the list of genes containing a domain of at least 150bp of said state within its gene body, using the genomic coordinates provided by Sequeira-Mendes et al.[37]. The proportion of genes of interest in that chromatin state was compared to the proportion of all nuclear genes in said state and the significance of the difference betwee the two proportions was examined using the Marascuilo procedure with a confidence level of 0.95. This procedure was performed using R code adapted from the NIST/SEMATECH tutorial (*NIST/SEMATECH e-Handbook of Statistical Methods*, Section 7.4.7.4, http://www.itl.nist.gov/div898/handbook/).

Declarations

Availability of data and material

All the RNA-Seq and ChIP-seq data are available at NCBI's Gene Expression Omnibus GEO Series accession number GSE244562.

Funding

This work was supported by the King Abdullah University of Science and Technology (KAUST) to Prof. Heribert Hirt.

Acknowledgments

We would like to thank the KAUST Bioscience Core labs for technical assistance for RNA sequencing.

Author contributions

HA, HH and NR designed the study. HA, SAM, DL, PM, AA, LF, OA, MA, FA, SA, SD, IB and NR performed experimental work. HA, AA, KM, DM, XH, FA JB, DP, DS, JC, WF, MB, SA, HH and NR performed *in silico* analysis and analyzed data. HA and NR wrote the paper. All co-authors read and approved the final manuscript.

Competing interests

The authors declare no conflict of interest regarding the publication of the present manuscript.

References

1. Jarillo, J. A., Piñeiro, M., Cubas, P. & Martínez-Zapater, J. M. Chromatin remodeling in plant development. Int J Dev Biol 53, 1581–1596 (2009). https://doi.org:10.1387/ijdb.072460jj
2. Chen, W., Zhu, Q., Liu, Y. & Zhang, Q. Chromatin Remodeling and Plant Immunity. Adv Protein Chem Struct Biol 106, 243–260 (2017). https://doi.org:10.1016/bs.apcsb.2016.08.006
3. Waldmann, T., Scholten, I., Kappes, F., Hu, H. G. & Knippers, R. The DEK protein–an abundant and ubiquitous constituent of mammalian chromatin. Gene 343, 1–9 (2004). https://doi.org:10.1016/j.gene.2004.08.029
4. Privette Vinnedge, L. M., Kappes, F., Nassar, N. & Wells, S. I. Stacking the DEK: from chromatin topology to cancer stem cells. Cell Cycle 12, 51–66 (2013). https://doi.org:10.4161/cc.23121
5. von Lindern, M. *et al.* Translocation t(6;9) in acute non-lymphocytic leukaemia results in the formation of a DEK-CAN fusion gene. Baillieres Clin Haematol 5, 857–879 (1992). https://doi.org:10.1016/s0950-3536(11)80049-1
6. Logan, G. E. *et al.* DEK oncogene expression during normal hematopoiesis and in Acute Myeloid Leukemia (AML). Blood Cells Mol Dis 54, 123–131 (2015). https://doi.org:10.1016/j.bcmd.2014.07.009
7. Piao, J. *et al.* High expression of DEK predicts poor prognosis of gastric adenocarcinoma. Diagn Pathol 9, 67 (2014). https://doi.org:10.1186/1746-1596-9-67
8. Wang, X. *et al.* High expression of oncoprotein DEK predicts poor prognosis of small cell lung cancer. Int J Clin Exp Pathol 7, 5016–5023 (2014).
9. Privette Vinnedge, L. M. *et al.* The DEK oncogene promotes cellular proliferation through paracrine Wnt signaling in Ron receptor-positive breast cancers. Oncogene 34, 2325–2336 (2015). https://doi.org:10.1038/onc.2014.173
10. Szer, I. S., Sierakowska, H. & Szer, W. A novel autoantibody to the putative oncoprotein DEK in pauciarticular onset juvenile rheumatoid arthritis. J Rheumatol 21, 2136–2142 (1994).
11. Sierakowska, H., Williams, K. R., Szer, I. S. & Szer, W. The putative oncoprotein DEK, part of a chimera protein associated with acute myeloid leukaemia, is an autoantigen in juvenile rheumatoid arthritis.

Clin Exp Immunol 94, 435–439 (1993). https://doi.org:10.1111/j.1365-2249.1993.tb08214.x

12. Mor-Vaknin, N. *et al.* DEK in the synovium of patients with juvenile idiopathic arthritis: characterization of DEK antibodies and posttranslational modification of the DEK autoantigen. Arthritis Rheum 63, 556–567 (2011). https://doi.org:10.1002/art.30138
13. Smith, E. A. *et al.* DEK is required for homologous recombination repair of DNA breaks. Sci Rep 7, 44662 (2017). https://doi.org:10.1038/srep44662
14. Devany, M., Kotharu, N. P. & Matsuo, H. Expression and isotopic labeling of structural domains of the human protein DEK. Protein Expr Purif 40, 244–247 (2005). https://doi.org:10.1016/j.pep.2004.07.008
15. Kappes, F., Scholten, I., Richter, N., Gruss, C. & Waldmann, T. Functional domains of the ubiquitous chromatin protein DEK. Mol Cell Biol 24, 6000–6010 (2004). https://doi.org:10.1128/mcb.24.13.6000-6010.2004
16. Kappes, F. *et al.* Phosphorylation by Protein Kinase CK2 Changes the DNA Binding Properties of the Human Chromatin Protein DEK. Molecular and Cellular Biology 24, 6011–6020 (2004). https://doi.org:10.1128/mcb.24.13.6011-6020.2004
17. Cleary, J. *et al.* p300/CBP-associated factor drives DEK into interchromatin granule clusters. J Biol Chem 280, 31760–31767 (2005). https://doi.org:10.1074/jbc.M500884200
18. Kappes, F. *et al.* DEK is a poly(ADP-ribose) acceptor in apoptosis and mediates resistance to genotoxic stress. Mol Cell Biol 28, 3245–3257 (2008). https://doi.org:10.1128/mcb.01921-07
19. Waldmann, T., Eckerich, C., Baack, M. & Gruss, C. The ubiquitous chromatin protein DEK alters the structure of DNA by introducing positive supercoils. J Biol Chem 277, 24988–24994 (2002). https://doi.org:10.1074/jbc.M204045200
20. Waldmann, T., Baack, M., Richter, N. & Gruss, C. Structure-specific binding of the proto-oncogene protein DEK to DNA. Nucleic Acids Res 31, 7003–7010 (2003). https://doi.org:10.1093/nar/gkg864
21. Soares, L. M., Zanier, K., Mackereth, C., Sattler, M. & Valcárcel, J. Intron removal requires proofreading of U2AF/3' splice site recognition by DEK. Science 312, 1961–1965 (2006). https://doi.org:10.1126/science.1128659
22. Le Hir, H., Izaurralde, E., Maquat, L. E. & Moore, M. J. The spliceosome deposits multiple proteins 20–24 nucleotides upstream of mRNA exon-exon junctions. Embo j 19, 6860–6869 (2000). https://doi.org:10.1093/emboj/19.24.6860
23. Alexiadis, V. *et al.* The protein encoded by the proto-oncogene DEK changes the topology of chromatin and reduces the efficiency of DNA replication in a chromatin-specific manner. Genes Dev 14, 1308–1312 (2000).
24. Kappes, F. *et al.* The DEK oncoprotein is a Su(var) that is essential to heterochromatin integrity. Genes Dev 25, 673–678 (2011). https://doi.org:10.1101/gad.2036411
25. Gamble, M. J. & Fisher, R. P. SET and PARP1 remove DEK from chromatin to permit access by the transcription machinery. Nat Struct Mol Biol 14, 548–555 (2007). https://doi.org:10.1038/nsmb1248

26. Ko, S. I. *et al.* Regulation of histone acetyltransferase activity of p300 and PCAF by proto-oncogene protein DEK. FEBS Lett 580, 3217–3222 (2006). https://doi.org:10.1016/j.febslet.2006.04.081
27. Hollenbach, A. D., McPherson, C. J., Mientjes, E. J., Iyengar, R. & Grosveld, G. Daxx and histone deacetylase II associate with chromatin through an interaction with core histones and the chromatin-associated protein Dek. J Cell Sci 115, 3319–3330 (2002). https://doi.org:10.1242/jcs.115.16.3319
28. Lee, K. S. *et al.* Caspase-dependent apoptosis induction by targeted expression of DEK in Drosophila involves histone acetylation inhibition. J Cell Biochem 103, 1283–1293 (2008). https://doi.org:10.1002/jcb.21511
29. Delaunay, S. *et al.* Elp3 links tRNA modification to IRES-dependent translation of LEF1 to sustain metastasis in breast cancer. J Exp Med 213, 2503–2523 (2016). https://doi.org:10.1084/jem.20160397
30. Hu, H. G., Scholten, I., Gruss, C. & Knippers, R. The distribution of the DEK protein in mammalian chromatin. Biochem Biophys Res Commun 358, 1008–1014 (2007). https://doi.org:10.1016/j.bbrc.2007.05.019
31. Ivanauskiene, K. *et al.* The PML-associated protein DEK regulates the balance of H3.3 loading on chromatin and is important for telomere integrity. Genome Res 24, 1584–1594 (2014). https://doi.org:10.1101/gr.173831.114
32. Sawatsubashi, S. *et al.* A histone chaperone, DEK, transcriptionally coactivates a nuclear receptor. Genes Dev 24, 159–170 (2010). https://doi.org:10.1101/gad.1857410
33. Kavanaugh, G. M. *et al.* The human DEK oncogene regulates DNA damage response signaling and repair. Nucleic Acids Res 39, 7465–7476 (2011). https://doi.org:10.1093/nar/gkr454
34. Deutzmann, A. *et al.* The human oncoprotein and chromatin architectural factor DEK counteracts DNA replication stress. Oncogene 34, 4270–4277 (2015). https://doi.org:10.1038/onc.2014.346
35. Waidmann, S., Kusenda, B., Mayerhofer, J., Mechtler, K. & Jonak, C. A DEK domain-containing protein modulates chromatin structure and function in Arabidopsis. Plant Cell 26, 4328–4344 (2014). https://doi.org:10.1105/tpc.114.129254
36. Waidmann, S. *et al.* GSK3-mediated phosphorylation of DEK3 regulates chromatin accessibility and stress tolerance in Arabidopsis. Febs j 289, 473–493 (2022). https://doi.org:10.1111/febs.16186
37. Zong, W. *et al.* DEK domain-containing proteins control flowering time in Arabidopsis. New Phytol 231, 182–192 (2021). https://doi.org:10.1111/nph.17366
38. Rayapuram, N. *et al.* Chromatin phosphoproteomics unravels a function for AT-hook motif nuclear localized protein AHL13 in PAMP-triggered immunity. Proc Natl Acad Sci U S A 118 (2021). https://doi.org:10.1073/pnas.2004670118
39. Nady, N. *et al.* Recognition of multivalent histone states associated with heterochromatin by UHRF1 protein. J Biol Chem 286, 24300–24311 (2011). https://doi.org:10.1074/jbc.M111.234104
40. Ruthenburg, A. J. *et al.* Recognition of a mononucleosomal histone modification pattern by BPTF via multivalent interactions. Cell 145, 692–706 (2011). https://doi.org:10.1016/j.cell.2011.03.053

41. Lu, Y. *et al.* A Chromodomain-Helicase-DNA-Binding Factor Functions in Chromatin Modification and Gene Regulation. Plant Physiol 183, 1035–1046 (2020). https://doi.org:10.1104/pp.20.00453
42. Sequeira-Mendes, J. *et al.* The Functional Topography of the Arabidopsis Genome Is Organized in a Reduced Number of Linear Motifs of Chromatin States. Plant Cell 26, 2351–2366 (2014). https://doi.org:10.1105/tpc.114.124578
43. Baerenfaller, K. *et al.* Diurnal changes in the histone H3 signature H3K9ac|H3K27ac|H3S28p are associated with diurnal gene expression in Arabidopsis. Plant Cell Environ 39, 2557–2569 (2016). https://doi.org:10.1111/pce.12811
44. Nishio, H., Nagano, A. J., Ito, T., Suzuki, Y. & Kudoh, H. Seasonal plasticity and diel stability of H3K27me3 in natural fluctuating environments. Nat Plants 6, 1091–1097 (2020). https://doi.org:10.1038/s41477-020-00757-1
45. Nejat, N., Rookes, J., Mantri, N. L. & Cahill, D. M. Plant-pathogen interactions: toward development of next-generation disease-resistant plants. Crit Rev Biotechnol 37, 229–237 (2017). https://doi.org:10.3109/07388551.2015.1134437
46. Bigeard, J. & Hirt, H. Nuclear Signaling of Plant MAPKs. Frontiers in Plant Science 9, 469 (2018). https://doi.org:10.3389/fpls.2018.00469
47. Latrasse, D. *et al.* MAPK-triggered chromatin reprogramming by histone deacetylase in plant innate immunity. Genome Biology 18, 131 (2017). https://doi.org:10.1186/s13059-017-1261-8
48. Panchy, N., Lehti-Shiu, M. & Shiu, S.-H. Evolution of Gene Duplication in Plants. Plant Physiology 171, 2294–2316 (2016). https://doi.org:10.1104/pp.16.00523
49. Cubas, P., Lauter, N., Doebley, J. & Coen, E. The TCP domain: a motif found in proteins regulating plant growth and development. Plant J 18, 215–222 (1999). https://doi.org:10.1046/j.1365-313x.1999.00444.x
50. Martín-Trillo, M. & Cubas, P. TCP genes: a family snapshot ten years later. Trends Plant Sci 15, 31–39 (2010). https://doi.org:10.1016/j.tplants.2009.11.003
51. Manassero, N. G., Viola, I. L., Welchen, E. & Gonzalez, D. H. TCP transcription factors: architectures of plant form. Biomol Concepts 4, 111–127 (2013). https://doi.org:10.1515/bmc-2012-0051
52. Navaud, O., Dabos, P., Carnus, E., Tremousaygue, D. & Hervé, C. TCP transcription factors predate the emergence of land plants. J Mol Evol 65, 23–33 (2007). https://doi.org:10.1007/s00239-006-0174-z
53. Howarth, D. G. & Donoghue, M. J. Phylogenetic analysis of the "ECE" (CYC/TB1) clade reveals duplications predating the core eudicots. Proc Natl Acad Sci U S A 103, 9101–9106 (2006). https://doi.org:10.1073/pnas.0602827103
54. Kosugi, S. & Ohashi, Y. DNA binding and dimerization specificity and potential targets for the TCP protein family. Plant J 30, 337–348 (2002). https://doi.org:10.1046/j.1365-313x.2002.01294.x
55. Mukhtar, M. S. *et al.* Independently evolved virulence effectors converge onto hubs in a plant immune system network. Science 333, 596–601 (2011). https://doi.org:10.1126/science.1203659

56. Kim, S. H. *et al.* The Arabidopsis immune adaptor SRFR1 interacts with TCP transcription factors that redundantly contribute to effector-triggered immunity. Plant J 78, 978–989 (2014). https://doi.org:10.1111/tpj.12527
57. Sugio, A., Kingdom, H. N., MacLean, A. M., Grieve, V. M. & Hogenhout, S. A. Phytoplasma protein effector SAP11 enhances insect vector reproduction by manipulating plant development and defense hormone biosynthesis. Proc Natl Acad Sci U S A 108, E1254-1263 (2011). https://doi.org:10.1073/pnas.1105664108
58. Danisman, S. *et al.* Arabidopsis class I and class II TCP transcription factors regulate jasmonic acid metabolism and leaf development antagonistically. Plant Physiol 159, 1511–1523 (2012). https://doi.org:10.1104/pp.112.200303
59. Guo, Z. *et al.* TCP1 modulates brassinosteroid biosynthesis by regulating the expression of the key biosynthetic gene DWARF4 in Arabidopsis thaliana. Plant Cell 22, 1161–1173 (2010). https://doi.org:10.1105/tpc.109.069203
60. Li, S. & Zachgo, S. TCP3 interacts with R2R3-MYB proteins, promotes flavonoid biosynthesis and negatively regulates the auxin response in Arabidopsis thaliana. Plant J 76, 901–913 (2013). https://doi.org:10.1111/tpj.12348
61. An, J., Guo, Z., Gou, X. & Li, J. TCP1 positively regulates the expression of DWF4 in Arabidopsis thaliana. Plant Signal Behav 6, 1117–1118 (2011). https://doi.org:10.4161/psb.6.8.15889
62. Nicolas, M. & Cubas, P. TCP factors: new kids on the signaling block. Curr Opin Plant Biol 33, 33–41 (2016). https://doi.org:10.1016/j.pbi.2016.05.006
63. Jacob, Y. *et al.* ATXR5 and ATXR6 are H3K27 monomethyltransferases required for chromatin structure and gene silencing. Nat Struct Mol Biol 16, 763–768 (2009). https://doi.org:10.1038/nsmb.1611
64. Mittelsten Scheid, O., Probst, A. V., Afsar, K. & Paszkowski, J. Two regulatory levels of transcriptional gene silencing in Arabidopsis. Proc Natl Acad Sci U S A 99, 13659–13662 (2002). https://doi.org:10.1073/pnas.202380499
65. Vaillant, I., Schubert, I., Tourmente, S. & Mathieu, O. MOM1 mediates DNA-methylation-independent silencing of repetitive sequences in Arabidopsis. EMBO Rep 7, 1273–1278 (2006). https://doi.org:10.1038/sj.embor.7400791
66. Kim, J. M., Sasaki, T., Ueda, M., Sako, K. & Seki, M. Chromatin changes in response to drought, salinity, heat, and cold stresses in plants. Front Plant Sci 6, 114 (2015). https://doi.org:10.3389/fpls.2015.00114
67. Luo, M. *et al.* Chromatin modifications and remodeling in plant abiotic stress responses. Biochim Biophys Acta 1819, 129–136 (2012). https://doi.org:10.1016/j.bbagrm.2011.06.008
68. Kouzarides, T. Chromatin modifications and their function. Cell 128, 693–705 (2007). https://doi.org:10.1016/j.cell.2007.02.005
69. Chen, M., Lv, S. & Meng, Y. Epigenetic performers in plants. Dev Growth Differ 52, 555–566 (2010). https://doi.org:10.1111/j.1440-169X.2010.01192.x

70. Zhang, X. in *Plant Genome Diversity Volume 1: Plant Genomes, their Residents, and their Evolutionary Dynamics* (eds Jonathan F. Wendel, Johann Greilhuber, Jaroslav Dolezel, & Ilia J. Leitch) 237–255 (Springer Vienna, 2012).
71. Jackson, J. P. *et al.* Dimethylation of histone H3 lysine 9 is a critical mark for DNA methylation and gene silencing in Arabidopsis thaliana. Chromosoma 112, 308–315 (2004). https://doi.org:10.1007/s00412-004-0275-7
72. Yun, M., Wu, J., Workman, J. L. & Li, B. Readers of histone modifications. Cell Res 21, 564–578 (2011). https://doi.org:10.1038/cr.2011.42
73. Lachner, M., O'Carroll, D., Rea, S., Mechtler, K. & Jenuwein, T. Methylation of histone H3 lysine 9 creates a binding site for HP1 proteins. Nature 410, 116–120 (2001). https://doi.org:10.1038/35065132
74. Bannister, A. J. *et al.* Selective recognition of methylated lysine 9 on histone H3 by the HP1 chromo domain. Nature 410, 120–124 (2001). https://doi.org:10.1038/35065138
75. Turck, F. *et al.* Arabidopsis TFL2/LHP1 specifically associates with genes marked by trimethylation of histone H3 lysine 27. PLoS Genet 3, e86 (2007). https://doi.org:10.1371/journal.pgen.0030086
76. Zhang, X. *et al.* The Arabidopsis LHP1 protein colocalizes with histone H3 Lys27 trimethylation. Nat Struct Mol Biol 14, 869–871 (2007). https://doi.org:10.1038/nsmb1283
77. Zhao, S. *et al.* Plant HP1 protein ADCP1 links multivalent H3K9 methylation readout to heterochromatin formation. Cell Research 29, 54–66 (2019). https://doi.org:10.1038/s41422-018-0104-9
78. Qian, S. *et al.* Dual recognition of H3K4me3 and H3K27me3 by a plant histone reader SHL. Nat Commun 9, 2425 (2018). https://doi.org:10.1038/s41467-018-04836-y
79. Yang, Z. *et al.* EBS is a bivalent histone reader that regulates floral phase transition in Arabidopsis. Nat Genet 50, 1247–1253 (2018). https://doi.org:10.1038/s41588-018-0187-8
80. Clough, S. J. & Bent, A. F. Floral dip: a simplified method for Agrobacterium-mediated transformation of Arabidopsis thaliana. Plant J 16, 735–743 (1998). https://doi.org:10.1046/j.1365-313x.1998.00343.x
81. Birkenbihl, R. P., Diezel, C. & Somssich, I. E. Arabidopsis WRKY33 is a key transcriptional regulator of hormonal and metabolic responses toward Botrytis cinerea infection. Plant Physiol 159, 266–285 (2012). https://doi.org:10.1104/pp.111.192641
82. Jefferson, R. A., Kavanagh, T. A. & Bevan, M. W. GUS fusions: beta-glucuronidase as a sensitive and versatile gene fusion marker in higher plants. Embo j 6, 3901–3907 (1987). https://doi.org:10.1002/j.1460-2075.1987.tb02730.x
83. Forcat, S., Bennett, M. H., Mansfield, J. W. & Grant, M. R. A rapid and robust method for simultaneously measuring changes in the phytohormones ABA, JA and SA in plants following biotic and abiotic stress. Plant Methods 4, 16 (2008). https://doi.org:10.1186/1746-4811-4-16
84. Almeida Trapp, M., De Souza, G. D., Rodrigues-Filho, E., Boland, W. & Mithofer, A. Validated method for phytohormone quantification in plants. Front Plant Sci 5, 417 (2014).

https://doi.org:10.3389/fpls.2014.00417

85. Andrews, S. (Babraham Bioinformatics, 2012).
86. Bolger, A. M., Lohse, M. & Usadel, B. Trimmomatic: a flexible trimmer for Illumina sequence data. Bioinformatics 30, 2114–2120 (2014). https://doi.org:10.1093/bioinformatics/btu170
87. Kim, D. *et al.* TopHat2: accurate alignment of transcriptomes in the presence of insertions, deletions and gene fusions. Genome Biology 14, R36 (2013). https://doi.org:10.1186/gb-2013-14-4-r36
88. Trapnell, C., Pachter, L. & Salzberg, S. L. TopHat: discovering splice junctions with RNA-Seq. Bioinformatics 25, 1105–1111 (2009). https://doi.org:10.1093/bioinformatics/btp120
89. Trapnell, C. *et al.* Differential gene and transcript expression analysis of RNA-seq experiments with TopHat and Cufflinks. Nature Protocols 7, 562 (2012). https://doi.org:10.1038/nprot.2012.016
90. Ramírez, F. *et al.* deepTools2: a next generation web server for deep-sequencing data analysis. Nucleic Acids Research 44, W160-W165 (2016). https://doi.org:10.1093/nar/gkw257
91. Liao, Y., Smyth, G. K. & Shi, W. featureCounts: an efficient general purpose program for assigning sequence reads to genomic features. Bioinformatics 30, 923–930 (2014). https://doi.org:10.1093/bioinformatics/btt656
92. Howe, E. A., Sinha, R., Schlauch, D. & Quackenbush, J. RNA-Seq analysis in MeV. Bioinformatics 27, 3209–3210 (2011). https://doi.org:10.1093/bioinformatics/btr490
93. Tian, T. *et al.* agriGO v2.0: a GO analysis toolkit for the agricultural community, 2017 update. Nucleic Acids Res 45, W122-w129 (2017). https://doi.org:10.1093/nar/gkx382
94. Aljedaani, F., Rayapuram, N. & Blilou, I. A Semi-In Vivo Transcriptional Assay to Dissect Plant Defense Regulatory Modules. Methods Mol Biol 2328, 203–214 (2021). https://doi.org:10.1007/978-1-0716-1534-8_13
95. Gendrel, A. V., Lippman, Z., Martienssen, R. & Colot, V. Profiling histone modification patterns in plants using genomic tiling microarrays. Nat Methods 2, 213–218 (2005). https://doi.org:10.1038/nmeth0305-213
96. Veluchamy, A. *et al.* LHP1 Regulates H3K27me3 Spreading and Shapes the Three-Dimensional Conformation of the Arabidopsis Genome. PLoS One 11, e0158936 (2016). https://doi.org:10.1371/journal.pone.0158936
97. Langmead, B., Trapnell, C., Pop, M. & Salzberg, S. L. Ultrafast and memory-efficient alignment of short DNA sequences to the human genome. Genome Biol 10, R25 (2009). https://doi.org:10.1186/gb-2009-10-3-r25
98. Lawrence, M. *et al.* Software for computing and annotating genomic ranges. PLoS Comput Biol 9, e1003118 (2013). https://doi.org:10.1371/journal.pcbi.1003118
99. Zhu, L. J. *et al.* ChIPpeakAnno: a Bioconductor package to annotate ChIP-seq and ChIP-chip data. BMC Bioinformatics 11, 237 (2010). https://doi.org:10.1186/1471-2105-11-237

Figures

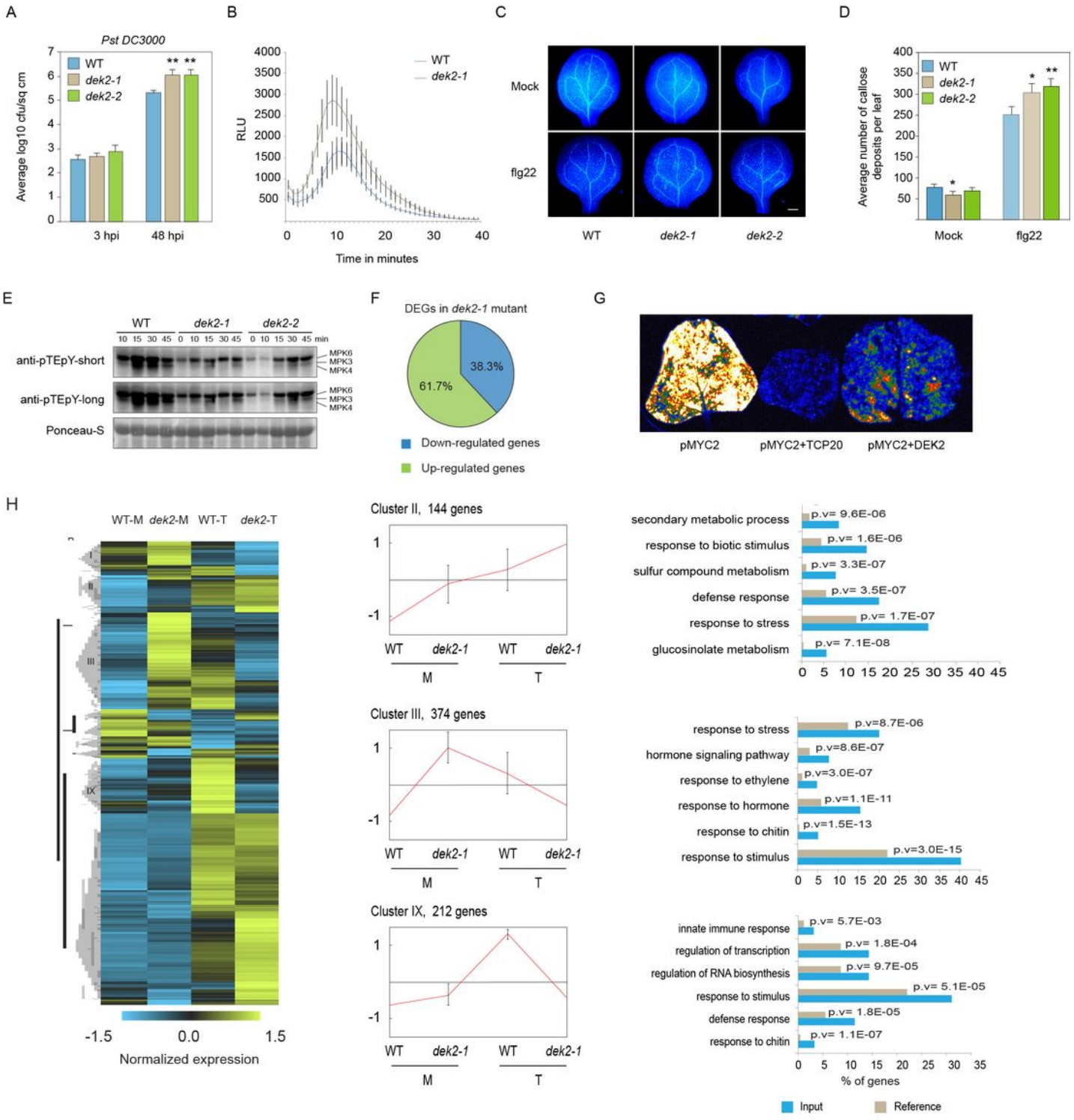

Figure 1

DEK2 regulates *A. thaliana* defense responses against *Pst* DC3000. A. Four-week-old plants were spray-infected with *P. syringae* pv. *tomato* (*Pst*) DC3000 with OD_{600}= 0.2. Bacterial numbers were counted after plating serial dilutions at the indicated time points. Values shown are means± SE (*n*=24) from three independent repetitions. **B**. ROS production was measured from WT and *dek2* mutant plants for 40 min after treatment with 1 µM of flg22. ROS production was quantified using a luminescence microplate

reader. Data are means ± SE and the experiments were repeated at least three times with similar results. The asterisks indicate statistically significant differences from the WT controls by Mann & Whitney U-test one tailed (*P < .05. **P < 0.01). **C** and **D**. Callose deposition in 14-day-old seedlings treated for 24 h with 1 µM flg22. Photographs of aniline blue-stained cotyledons under UV fluorescence were quantified with ImageJ. Data shown are mean values ± SE from three independent biological replicates (*n*=12). **E**. flg22 induced MAPK activation in WT, *dek2-1* and *dek2-2* plants. **F**. Pie chart reveals the percentage of up- and down-regulated genes in *dek2-1* mutant. **G.** Transcriptional repression activity of DEK2 measured by Dual luciferase system in tobacco leaves. pMYC2 was fused to firefly luciferase and expressed under a CaMV 35S promoter with RFP fusion. Luminescence was measured using a CCD Luminescence camera. TCP20 was used a positive control. **H.** Heat map depicting differential expression profiles in WT and *dek2* plants at 24 h post hrcC- inoculation or mock treatment (fold change ≥ 2, P value ≤ 0.05). The original fragments per kilobases million values were subjected to data adjustment by normalizing genes or rows and hierarchical clustering was generated with the average linkage method using MeV4.0. C) Selection of three clusters displaying interesting gene ontology from the heatmap comparisons are shown. GO terms were identified using the AgriGO v2.0 Term Enrichment Tool.

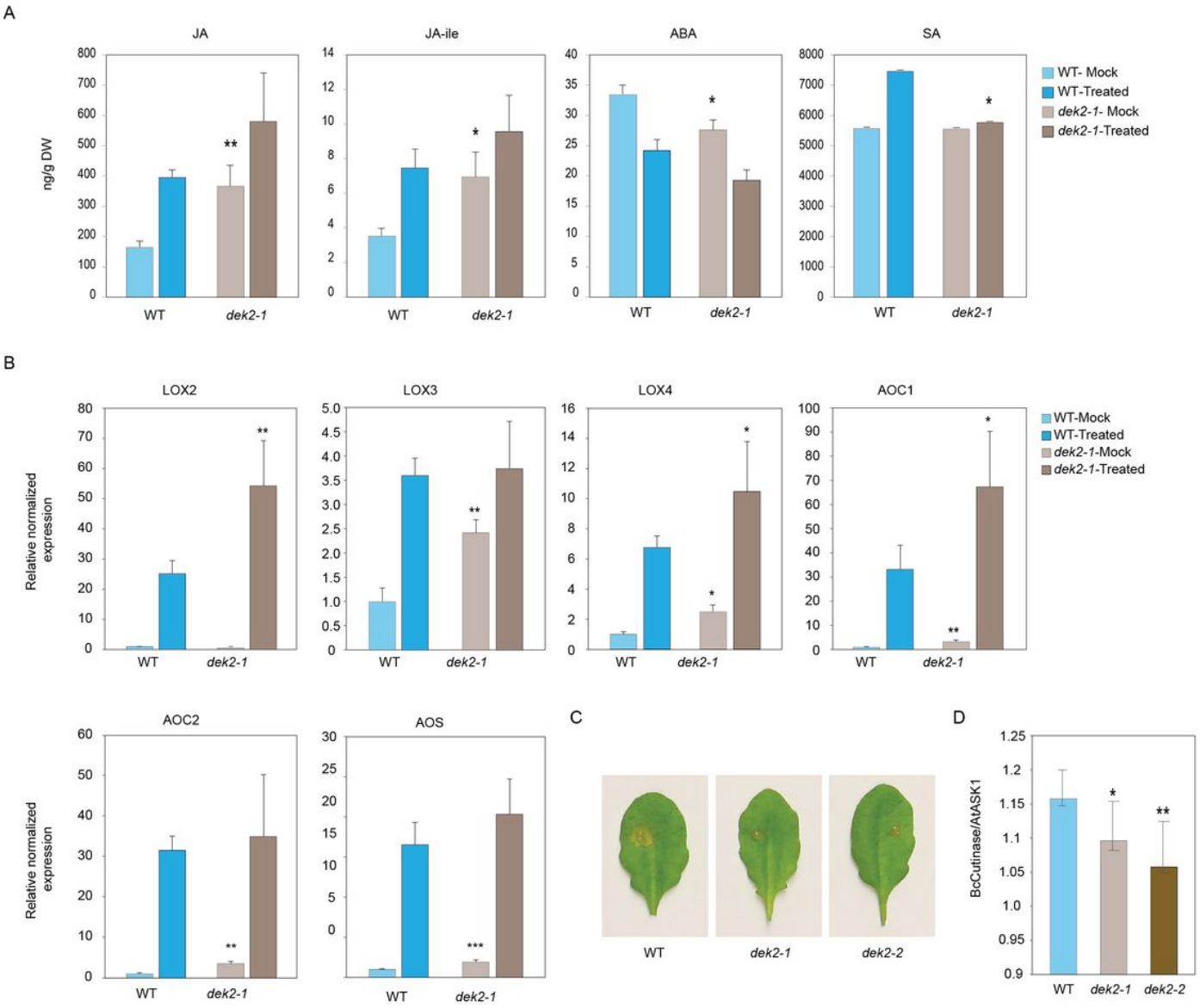

Figure 2

Hormone quantification in the WT and *dek2-1* mutant. **A**. The levels of JA, JA-Ile, ABA and SA defense hormones measured in WT and *dek2-1* mutant plants at 24 hpi with hrcC- or mock. Data represent the means of six biological replicates. **B**. qPCR analysis of the expression of JA marker genes involved in biosynthesis pathway. Expression of *Ubi* and *Actin* genes were used for normalization, and fold induction values of all genes were calculated relative to the expression level of mock WT plants. Error bars represent SE. The asterisks indicate statistically significant differences from the WT controls by Biorad CFX software at $p \leq 0.05$. **C**. Four-week-old leaves from WT and *dek-2* mutant plants were drop-inoculated with $5x10^5$ spores/ml of *B. cinerea*. The diameter of the lesion area was measured 2 days after inoculation by imageJ. **D**. Ratio of *Bc* cutinase gene over *A. thaliana* ASK1 gene by qPCR analysis. Values shown are means ± SE (*n*=15) from three independent repetitions.

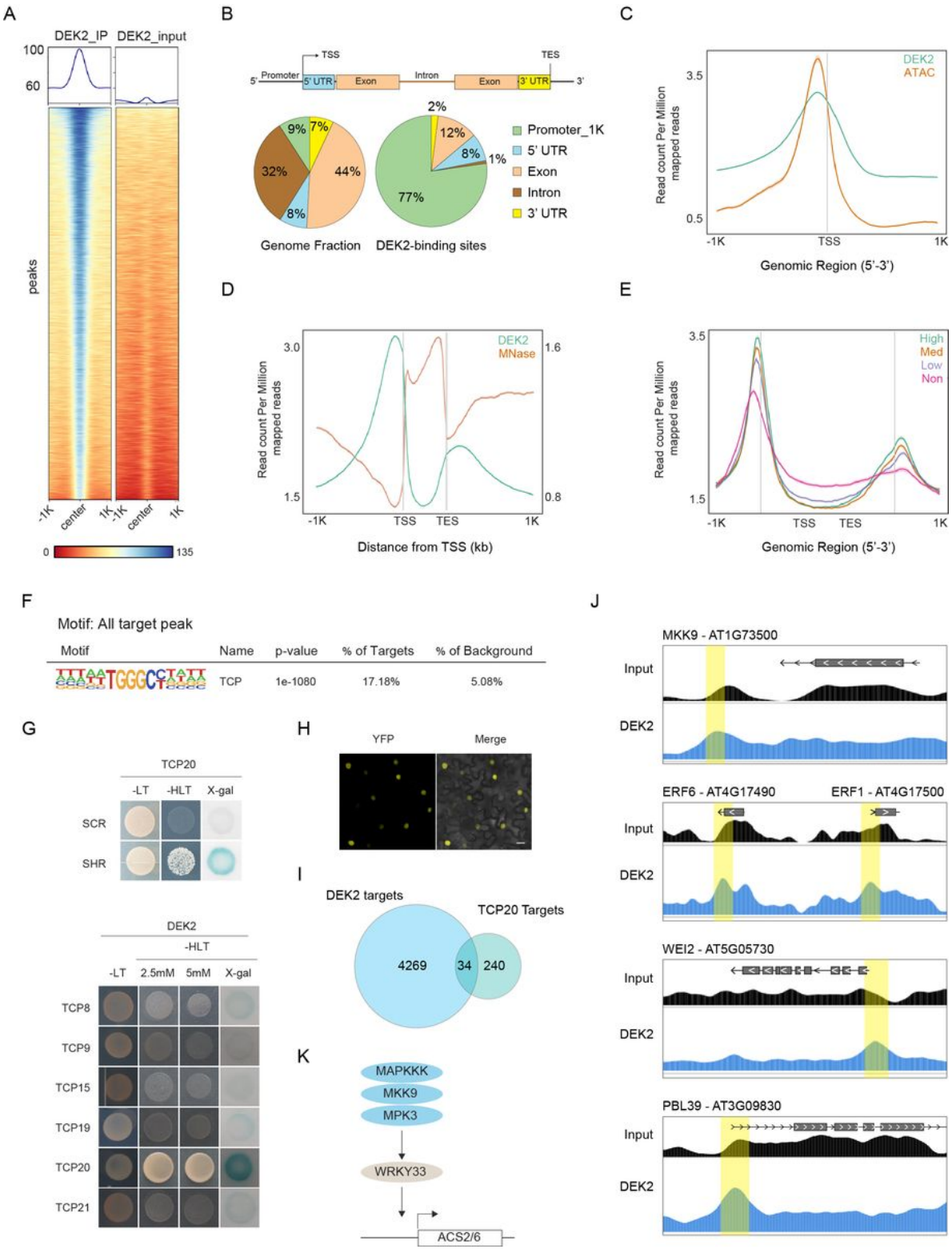

Figure 3

DEK2 binds the promoter regions of genes. **A**. ChIP-seq was performed on 14-days-old seedlings expressing DEK2-YFP under it's the native promoter. Comparison of heatmaps between DEK2 IP and input in the regions ±1 kb around the DEK2 peaks. **B**. Pie chart representation of the distribution of DEK2 peaks identified by ChIP-seq in five genomics regions depicted in the schematic diagram showing the Transcription Start Site (TSS) and the Transcription End Site (TES). **C**. Merged profiles of DEK2 ChIP-seq

and ATAC-seq read density over TSS and flanking 1-kb region. **D**. Mean profile of DEK2 ChIP-seq and MNase-seq read density with respect to a gene model from TSS to TES. Normalization of coverage using spline algorithm was performed over the genes and flanking 1-kb region. **E**. Average enrichment profile of DEK2 is correlated with gene expression variation. Gene expression is categorized from low (first quantile) to high (fourth quantile) expression. Mean-normalized ChIP-seq densities of equal bins along the gene and 1-kb region flanking the TSS or the TES are plotted. Highly expressed genes show higher enrichment for binding of DEK2. **G**. Y2H with Class 1 TCPs. **H**. BiFC with TCP20. **I**. Overlap of DEK2 and TCP20 targets. **J**. Screen shots of several potential DEK2 target genes reveals a high enrichment for genes involved in hormone biosynthesis and signaling, transcription factors and defense response. The upper panel represents the input control sample while the lower enrichment represents the DEK2-YFP IP sample. The gene structures are shown at the top of each panel. **K**. The pathway involved in ET biosynthesis.

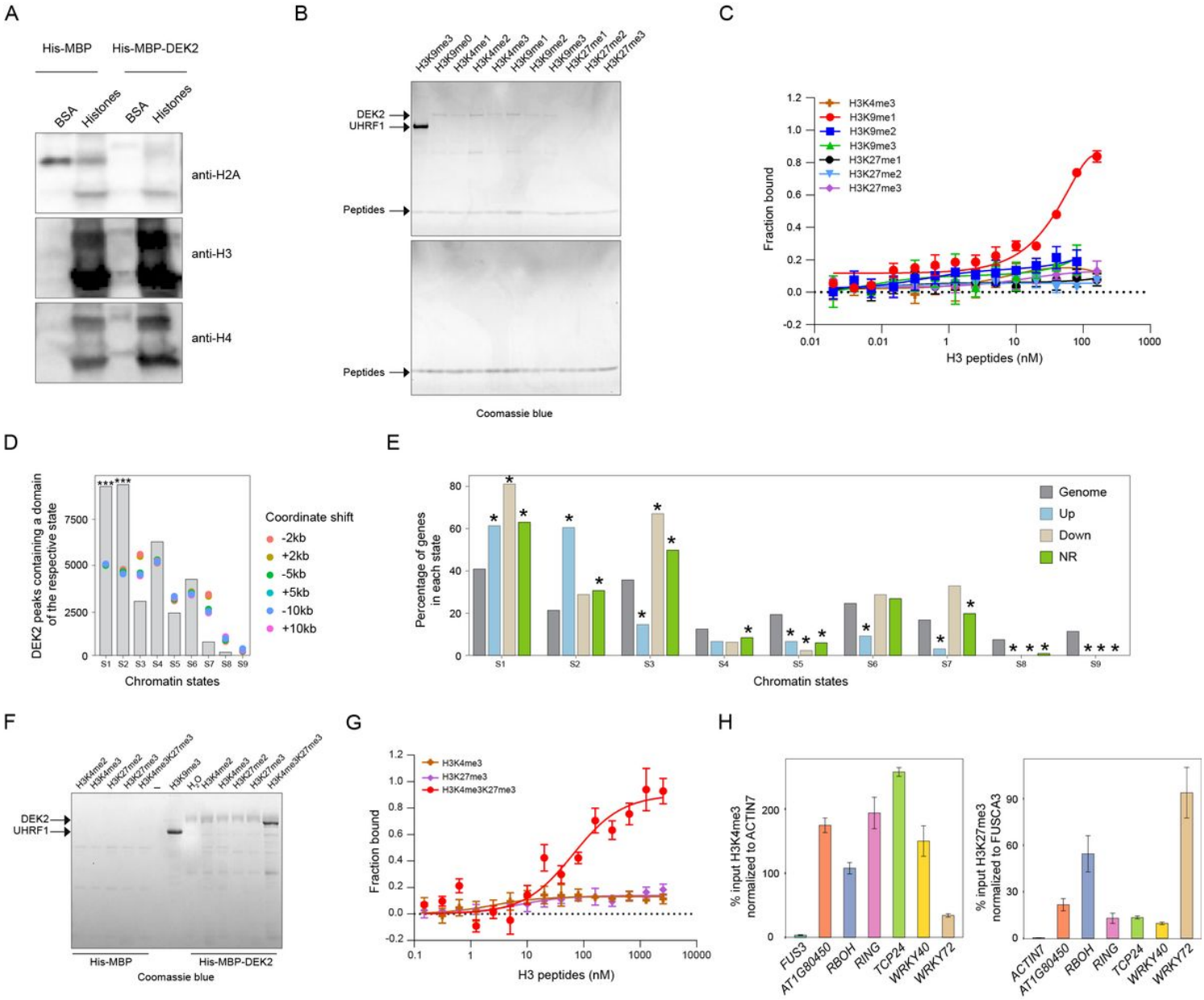

Figure 4

DEK2 is a reader of bivalent histone marks. A. Purified recombinant His-MBP-DEK2 binds histone H3 and H4 in a pull-down assay. After incubating the Ni-NTA beads bound His-MBP-DEK2 wicalf thymus histones, the proteins were resolved by SDS-PAGE and probed with antibodies against H2A, H3 and H4. B. Histone H3 modified peptide pull-down with His-MBP-DEK2. Biotinylated modified H3 peptides were bound to streptavidin beads and then incubated with purified His-MBP-DEK2 protein, resolved by SDS-PAGE and stained with Coomassie Brilliant blue stain. C. The interaction between His6-MBP-DEK2 and modified H3 peptides by MST. The negative control shows the interaction between His6-MBP and H3K9 peptides. MST binding experiments were carried out at LED: 40% Power: 40%. The dissociation constant (Kd) is shown. Data represent the mean +/− SD of at least three technical replicates. D. Number of DEK2 peaks containing a domain of each of the indicated states. The states coordinates were obtained from Sequeira et al. (2014). The ±2 kb, ± 5 kb and ±10 kb are control sets where the coordinates of the DEK2 peaks were shifted up- (+) or downstream (-) by the indicated number of bases. Significance was tested by permutation test, *** indicate p-value ≤ 0.001. E. Chromatin state analysis of the DEK2 target genes. The states coordinates were obtained from Sequeira et al. (2014). The DEK2 target genes were divided into three categories: upregulated, downregulated and non-regulated based on their expression level in the RNA-seq dataset. * indicates significance compared to the genome, tested by Marascuilo procedure (α= 0.05). F. Histone H3 bivalent modified peptide pull-down with His-MBP-DEK2. Biotinylated modified H3 peptides H3K4me2, H3K4me3, H3K27me2, H3K27me3 and H3K4me3K27me3 were bound to streptavidin beads and then incubated with purified His-MBP-DEK2 protein, resolved by SDS-PAGE and stained with Coomassie Brilliant blue stain. G. The interaction between His6-MBP-DEK2 and modified H3K4me3, H3K27me3 and H3K4me3K27me3 peptides by MST. MST binding experiments were carried out at LED: 40% Power: 40%. The dissociation constant (Kd) is shown. H. ChIP-PCR of a few target genes after IP with H3K4me3 (normalized to ACTIN7) and H3K27me3 (normalized to FUSCA3).

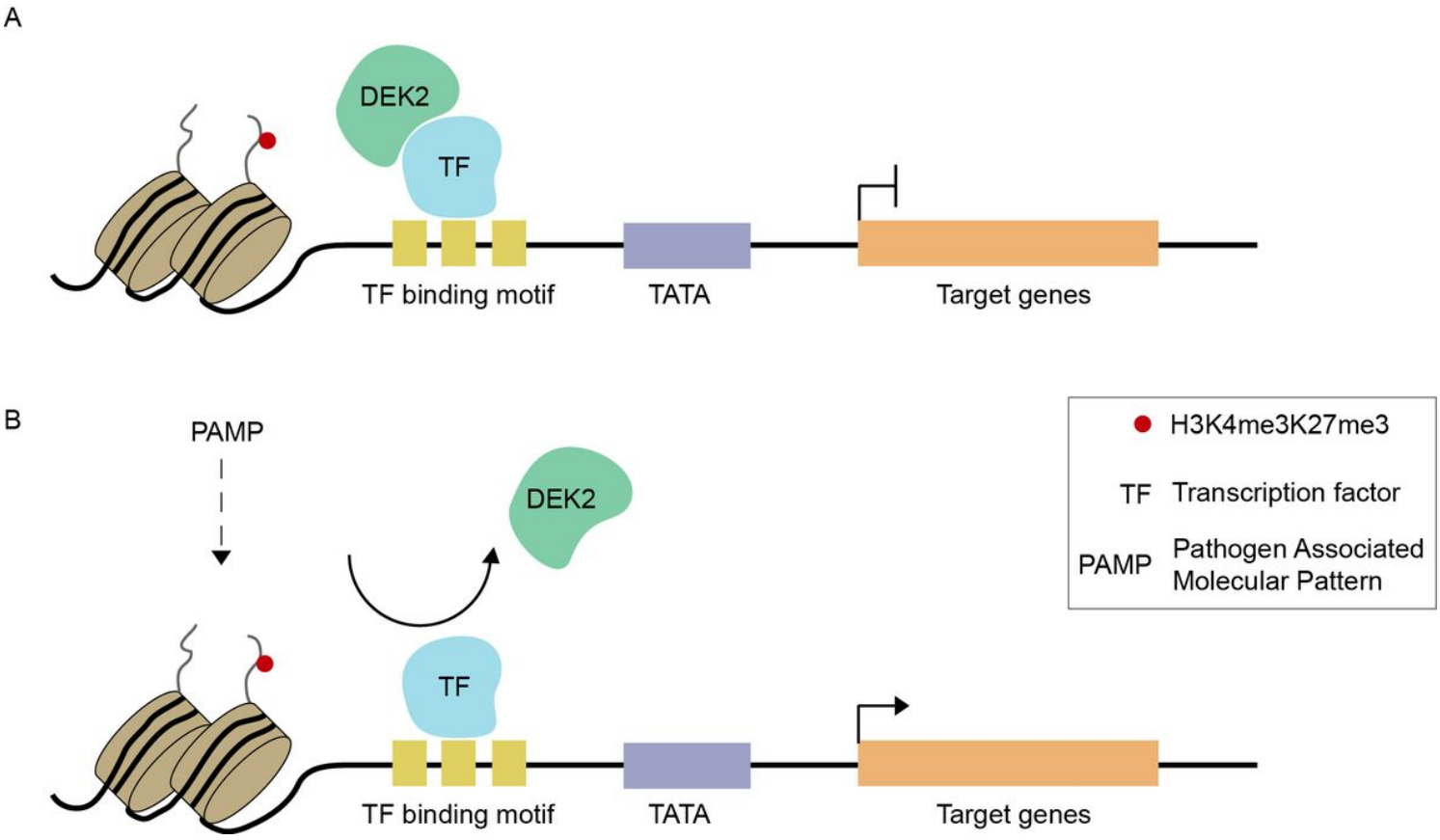

Figure 5

Hypothetical working model for DEK2 function. A. Unstressed conditions**. B.** after PAMP treatment.

Supplementary Files

This is a list of supplementary files associated with this preprint. Click to download.

- TableS1RNAseqDEGs.xlsx
- TableS2DEK2targetgenesChIP.xlsx
- TableS3Primersusedinthisstudy.xlsx
- SupplementaryFigures.docx